Hindawi
Advances in Meteorology
Volume 2018, Article ID 1747530, 9 pages
https://doi.org/10.1155/2018/1747530

Review Article

The Application of Barnes Filter to Positioning the Center of Landed Tropical Cyclone in Numerical Models

Haibo Zou,[1] **Shanshan Wu**,[2] **Xueting Yi**,[1] **and Nan Wu**[1]

[1]*Meteorological Disaster Emergency Warning Centre of Jiangxi, Nanchang 330096, China*
[2]*Jiangxi Climate Centre, Nanchang 330096, China*

Correspondence should be addressed to Shanshan Wu; pilgrim_@163.com

Received 17 September 2017; Revised 27 December 2017; Accepted 18 January 2018; Published 13 February 2018

Academic Editor: Hisayuki Kubota

After a tropical cyclone (TC) making landfall, the numerical model output sea level pressure (SLP) presents many small-scale perturbations which significantly influence the positioning of the TC center. To fix the problem, Barnes filter with weighting parameters $C = 2500$ and $G = 0.35$ is used to remove these perturbations. A case study of TC Fung-Wong which landed China in 2008 shows that Barnes filter not only cleanly removes these perturbations, but also well preserves the TC signals. Meanwhile, the centers (track) obtained from SLP processed with Barnes filter are much closer to the observations than that from SLP without Barnes filter. Based on the distance difference (DD) between the TC center determined by SLP with/without Barnes filter and observation, statistics analysis of 12 TCs which landed China during 2005–2015 shows that in most cases (about 85%) the DDs are small (between −30 km and 30 km), while in a few cases (about 15%) the DDs are large (greater than 30 km even 70 km). This further verifies that the TC centers identified from SLP with Barnes filter are more accurate compared to that directly obtained from model output SLP. Moreover, the TC track identified with Barnes filter is much smoother than that without Barnes filter.

1. Introduction

Positioning the rotational center of an existing tropical cyclone (TC) not only significantly influences the forecast of TC precipitation and track [1], but also impacts the estimate of TC intensity [2] which is an important factor to assess risk for emergency managers and analyze potential losses for insurance and business interests [3]. Therefore, finding the TC center is an essential step in the analysis and forecast of the event [4], and one of the most important works on the research and operational forecast for TC [5]. An accurate positioning of TC center is also the need of track predictions in numerical model because the initial condition of model relies on the synthetic (bogus) TC [6] and initial TC motion vectors [7].

At present, many meteorologists have done a series of researches on positioning TC center from satellite data [4, 8], GPS and sounding data [9], and Doppler radar data [10–15]. For instance, Liu et al. [8] designed a method to determine the TC center using cloud derived wind vectors based on the characteristic that TC has small spin and large translation motion. Wimmers and Velden [4] constructed an objective algorithm for positioning TC center using satellite images and the brightness temperature gradient in spiral direction. A method based on the down projection sounding and aircraft observation was designed by Kepert [9] for finding TC center. With radar radial vectors, Wood [10] developed a geometric positioning method to locate TC center which have the characteristic of symmetrical and uniform wind speed distribution. On this basis, many meteorologists [11, 12, 14] improved this method and decreased the influence of TC asymmetry on positioning TC center, effectively elevating the accuracy of positioning TC center. In addition to radar radial velocity, radar reflectivity is also used to determine the TC center [13, 15]. In these data, satellites have significant advantage to position TC center because it has continuous monitoring ability and large coverage (especial over the oceans). Therefore, operationally issuing agencies of TC best-track datasets, such as The China Meteorological Administration (CMA) [16], the National Hurricane Center (NHC) [17], the Joint Typhoon Warning Center (JTWC) [17], and the Air Force Weather Agency (AFWA) [18], identify the

location and intensity of a TC mainly based on the Dovrak method [19–21]. This method identifies the location of TC by analyzing satellite image patterns and infrared cloud-top temperature [17, 21].

In high-resolution numerical models, TC centers can only be determined by model outputs themselves. Several methods of positioning the TC center from numerical model data are developed. For example, Li [22], Shuixin et al. [23], and Cruz and Narisma [24] defined the TC center as the position of the lowest SLP. Fiorino et al. [25] and Hsiao et al. [26] used maximum relative vorticity at low-level to identify the TC center. Heming et al. [27] used maximum relative vorticity at 850 hPa greater than 5.5×10^{-5} s^{-1} to search TC in the UK Meteorological Office Model. Liou and Sashegyi [28] searched the TC center by checking 850 hPa wind directions. Cavallo et al. (2013) defined the TC center as the location that maximized the 800 hPa circulation over a circle of 150 km radius. Actually, this method is similar to that of Fiorino et al. [25] and Hsiao et al. [26] because the circulation about a closed loop divided by the area enclosed equals the relative vorticity within the area enclosed [29]. Reasor and Montgoemery (2001) used the centroid of potential vorticity within a predetermined box as the TC center. Based on the method of Reasor and Montgoemery (2001), Riemer et al. (2010) defined the TC center using relative vorticity instead of potential vorticity. Nguyen et al. [29] discovered that the centroid pressure method, which was applied in Geophysical Fluid Dynamics Laboratory (GFDL) Hurricane Prediction System to determine TC center [30], can identify the TC center within the region of weak-relative wind and produce a smooth track. Besides, Lord and Petersen [31] used a combination of minimum geopotential height, minimum wind speed, and maximum relative vorticity at 850 hPa to detect TC center. Walsh [32] developed an automated procedure based on several different parameters (maximum vorticity, minimum pressure, maximum 10 m wind speed, minimum total tropospheric temperature anomaly, mean wind speed difference between 850 hPa and 300 hPa, and the temperature difference between 850 hPa and 300 hPa) to detect TC in high-resolution analyses from European Centre for Medium-Range Weather Forecasts.

These methods mentioned above perform well to find the location of TC center in practice. But when TC landed mainland, its intensity rapidly weakens due to the large friction and the reduction of water vapor supply. In the presence of heterogeneous land surface, these parameters such as SLP, vorticity, wind speed, and geopotential height usually contain small-scale perturbations and present multiple large or small centers around the true TC center. Therefore, directly using these methods mentioned above to identify TC center may find pseudo TC center. The automated procedure developed by Walsh [32] also does not search points over the land. In the centroid method of vorticity or pressure, the centroid was calculated based on the first guess of TC center which is defined as the location of minimum pressure on a constant height surface [29]. Thus, using the centroid method to identify landed TC center was also affected by small-scale perturbation.

It is clear that the presence of small-scale perturbation in SLP (wind, vorticity, geopotential height, etc.) field has significant effect on correctly identifying the center of landed TC in a numerical model. Therefore, removing the small-scale perturbation from the model output fields (such as SLP and vorticity) is favorable for improving the accuracy of TC center determined by the above methods. Barnes [33] developed a 2D space filter (Barnes filter) based on Gaussian weighting function to separate different scale signals from the raw field. Barnes [34] and Doswell [35] further improved the filter to reduce the computational time. Barnes filter is widespread applied to 2D signal separation and 2D data interpolation since it was developed. For example, Gomis and Alonso [36] quantitatively extracted the large-scale and mesoscale signals from geopotential height, temperature and wind fields using Barnes filter and then analyzed the interaction of different scales in Mediterranean cyclogenesis occurring in 1982. Hong et al. [37] successfully extracted southwest China vortex signals with wavelength between 300 and 800 km from National Centers for Environmental Prediction (NCEP) data using Barnes filter. In order to diagnose extratropical cyclones over the central United States, Morris (2001) interpolated the observational station data into grid data and removed the information with wavelengths less than 500 km using Barnes filter. Askelson et al. [38] showed that the Barnes filter may be preferable on processing radar data compared to Cressman filter due to the easy computation of the response function of Barnes filter. In view of well performance of Barnes filter, this paper aims to address the positioning issue of landed TC in numerical model by removing small-scale perturbation using Barnes filter. Section 2 introduces the data and the proposition of problem for positioning landed TC center. Section 3 describes Barnes filter and its application in a case and Section 4 shows its performance in statistical analysis. Conclusions are given in Section 5.

2. Data and Problem

2.1. Data. The TC best-track data in the present study is provided by CMA tropical weather data center (http://tcdata.typhoon.org.cn/). The 6-hour dataset includes the ID, location (latitude and longitude), date/time, minimum SLP, and maximum wind speed of TCs [16]. Moreover, the Final (FNL) Operational Global Analyses from Global Forecast System (GFS) with 6 h temporal- and 1° spatial-resolutions are used as the initial and boundary conditions for the Weather Research Forecast (WRF) model. In order to perform statistical analysis, these data for a 12-year period from 1 January 2005 to 31 December 2016 were selected.

2.2. The Proposition of Problem. Figure 1 shows the distribution of the SLP, 850 hPa geopotential height, 850 hPa relative vorticity, and 850 hPa potential vorticity simulated by WRF model at 1200 UTC 30 July 2008 after the TC Fung-Wong landed China. The configure of WRF model is as follows: a single domain centered at point (116°E, 26.5°N) with a horizontal grid spacing of 12 km is chosen; the model grid comprises $291 \times 291 \times 40$ points; the model top is set to 50 hPa, and the output interval is 3 h; cumulus parameterization scheme is set to the Betts-Miller-Janjic (BMJ) scheme and cloud microphysics scheme is set to the Lin scheme; the simulation with a 60 s time step starts from 1200 UTC 28

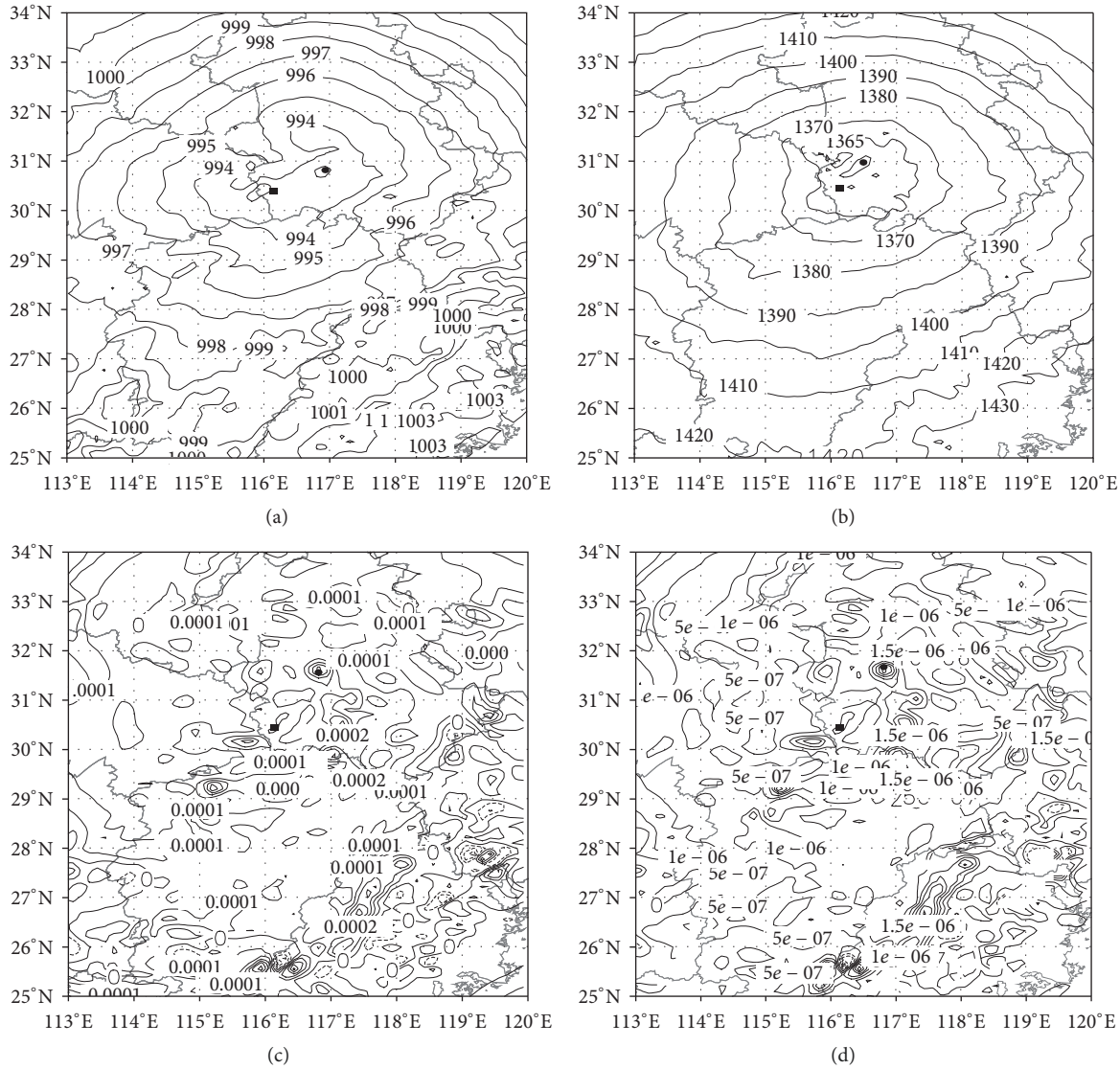

Figure 1: The sea level surface pressure ((a), hPa), 850 hPa geopotential height ((b), gpm), relative vorticity ((c), s^{-1}), and potential height ((d), $m^2 \cdot K \cdot s^{-1} \cdot kg^{-1}$) simulated by WRF model at 1200 UTC 30 July 2008. The filled square represented the observed TC center and the filled circle indicated the point with minimum value (in (a) and (b)) or maximum value (in (c) and (d)) around observed TC center.

to 1200 UTC 30 July 2008. As shown in Figures 1(a) and 1(b), when TC Fung-Wong landed China, it weakened rapidly with central pressure (height) increased to about 993 hPa (1360 gpm) owing to the increased surface friction and the reduced water vapor supply. In the action of uneven underlying surface of Chinese mainland, small-scale perturbation with wavelength less than 100 km appeared at SLP field and 850 hPa geopotential height field around observed TC center. In this case, these small-scale perturbations result in a significant deviation (more than 70 km distance) of the simulated TC center (filled circle), which is positioned by the point with minimum SLP or minimum geopotential height around observed TC center, from the observed TC center (filled square). The TC center identified by SLP (geopotential height) locates at the east (north) instead of the center of main body of TC Fung-Wong. Interestingly, the 850 hPa vorticity and potential vorticity have similar distribution in which there are no obviously TC signals (Figures 1(c) and 1(d), more small-scale signals). Many maximum centers distribute all over the whole domain and the TC center determined by maximum vorticity (potential vorticity) deviates about 150 km from the observed TC center. It is clear that the direct use of the SLP, geopotential height, vorticity, and potential vorticity to determine landed TC center may result in large deviation or error due to the presence of small-scale perturbations. Additionally, using SLP or geopotential height at 850 hPa to identify the landed TC's center in numerical models has obvious advantages compared to that using relative vorticity or potential vorticity at 850 hPa.

3. Barnes Filter

The above analysis shows that there are many small-scale perturbations appearing in the numerical simulated SLP and

geopotential height after TC making landfall, and they often result in the failure of identifying TC center by using the lowest SLP or geopotential height at 850 hPa. Therefore, if these small-scale perturbations are removed using Banes filter in SLP and geopotential height, the TC center is expected to be correctly found.

3.1. Introduction to Barnes Filter. Under the assumption that the distribution of an atmospheric variable can be depicted by a Fourier integral, Barnes [33] developed a filter based on Gaussian weighting function to interpolate and filter a 2D variable. Then, Barnes [34] and Doswell [35] modified the filter and made it only need one iteration rather than several successive iterations and significantly reduced the computational time. It has shown excellent performance in separating different signals of different scales from a 2D meteorological field [35–37]; (Morris 2001). Therefore, the Barnes filter will be selected in the present study to remove the small-scale perturbations in numerical simulated variables to improve the accuracy of simulated TC center. The expressions of modified Barnes filter [34–37] are as follows:

$$F_0(x,y) = \frac{\sum_{k=1}^{M} w_k F(x_k, y_k)}{\sum_{k=1}^{M} w_k}, \tag{1}$$

$$w_k = \exp\left(-\frac{r_k^2}{4C}\right), \tag{2}$$

$$F_1(x,y) = F_0(x,y) + \frac{\sum_{k=1}^{M} w_k' \left(F(x_k, y_k) - F_0(x_k, y_k)\right)}{\sum_{k=1}^{M} w_k'}, \tag{3}$$

$$w_k' = \exp\left(-\frac{r_k^2}{4GC}\right), \tag{4}$$

where $F(x, y)$ is the simulated variable (like SLP, geopotential height, etc.) by WRF model, $F_0(x, y)$ is the initial filter value of $F(x, y)$, $F_1(x, y)$ is the final filter value of $F(x, y)$, M is the grid numbers within an influence range (generally 120 km) of the grid point (x, y), w_k is the Gaussian weight function, w_k' is the modified Gaussian weight function by Barnes [34], C and G are the filter coefficient, and r_k is the distance between point (x, y) and point (x_k, y_k), which can be calculated by the formula of spherical distance between two points on the earth:

$$r_k = R \arccos\left(\cos\varphi \cos\varphi_k \cos(\theta - \theta_k) + \sin\varphi \cos\varphi_k\right), \tag{5}$$

where θ and φ are, respectively, the longitude and latitude of grid point (x, y) and θ_k and φ_k, respectively, the longitude and latitude of grid point (x_k, y_k). $R = 6370$ km is the earth's radius. Since (2) approaches zero asymptotically as C increases, the influence of data may be extended to any distance without changing the weight function and response characteristics (Maddox 1980).

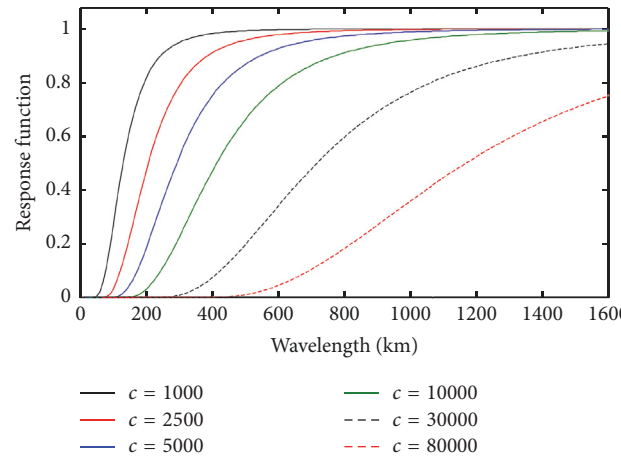

Figure 2: The response function of Barnes filter for different parameters C when $G = 0.35$.

3.2. Selection of Filter Coefficients. Barnes [34] and Maddox (1980) indicated that, prior to performing the Barnes filter, the weighting function coefficients C and G in (2) and (4) should be chosen so that pattern scales resolvable by the data distribution will be revealed to known response amplitude. The response of Barnes filter, which is defined as the ratio of the amplitude in output signals to that of input, is a function of wavelength λ and is expressed as ([36]; Maddox 1980)

$$R_1 = R_0\left(1 + R_0^{G-1} - R_0^{G}\right), \quad R_0 = \exp\left(-\frac{4\pi^2 C}{\lambda^2}\right). \tag{6}$$

The larger the response R_1, the more retainment of the signals in the variable field for the corresponding wavelength and vice versa. Approaching 0 of the response R_1 indicates that the signals of the corresponding wavelength are completely removed. In contrast, R_1 approaching 1 represents that the signals of corresponding wavelength are totally preserved. Generally, $R_1 > 0.5$ (<0.5) indicates the signals of corresponding wavelength are basically retained (removed) in the field [36, 37]. Equations (6) show that the responses of Barnes filter are only determined by coefficient C and G in a certain wavelength. The coefficient G is greater than 0 and less than 1 ([34] and Maddox 1980). When $G > 0.5$, the response function is difficult to converge fast, and $G = 0.35$ is a widespread choice in practice ([36, 37]; Maddox 1980). Therefore, in the present study the coefficient G is also set to 0.35.

Different response curves with wavelength at different values of C are shown in Figure 2. The response increases with the wavelength in a given C. The corresponding wavelength of response function at 0.5 rapidly increases with the increase of parameter C, implying that the larger C is, the longer wavelength of the signal is removed. Meanwhile, given a wavelength the response rapidly decreases with the raise of C. It is also shown in Figure 2 that when the wavelength is 100 km, the response with $C = 1000$ ($C = 2500$) is close to 0.5 (0.1). This indicates that the signals with wavelength less than 100 km, which significantly affected the positioning of landed

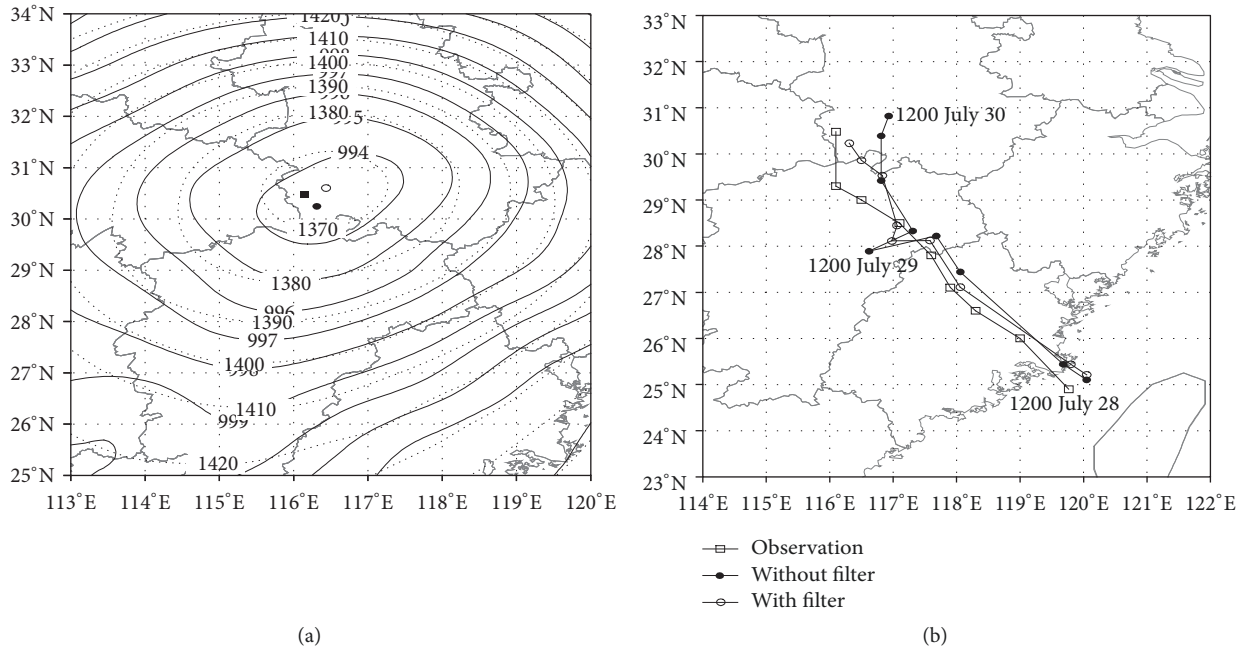

Figure 3: (a) The simulated sea level pressure (solid line, unit hPa) and 850 hPa geopotential height (dotted line, unit gpm) filtered by Barnes filter at 1200 UTC 30 July 2008, and the filled (open) circle indicates the TC center determined by lowest SLP (geopotential height) while the filled square represents the observed TC center. (b) The observed track (observation), the track determined by SLP with Barnes filter (with filter), and the track determined by SLP without Barnes filter (without filter) for TC Fung-Wong after landing China mainland.

TC center in numerical models, are basically preserved (mostly removed) at $C = 1000$ ($C = 2500$). In addition, the response with $C = 2500$ is about 0.8 at 300 km wavelength, implying that the substantial signals of wavelength more than 300 km are preserved. Generally, the radius of TC exceeds 150 km. In other words, the wavelength corresponding to the TC signal is more than 300 km (double the TC radius). Therefore, selecting $C = 2500$ is very appropriate in the present study because the Barnes filter can not only cleanly remove the perturbation with wavelength less than 100 km, but also commendably preserve the TC signals.

4. Results

4.1. Case Study. After removing small-scale perturbations based on the Barnes filter with $C = 2500$ and $G = 0.35$, the distribution of simulated sea level pressure and 850 hPa geopotential height at 1200 UTC 30 July 2008 are depicted in Figure 3(a). There is hardly small-scale perturbation with wavelength less than 100 km in SLP and 850 hPa geopotential height fields in which the TC signals (low pressure system) are perfectly expressed. This verifies the well performance of the Barnes filter in scale separation. As also shown in Figure 3(a), the isolines of SLP almost overlap at that of 850 hPa geopotential height on 1200 UTC 30 July 2008, indicating that the SLP and 850 hPa geopotential height processed by Barnes filter accurately describes the TC system. Besides, the TC center determined by filtered SLP or 850 hPa geopotential height based on the method of the lowest SLP is much closer to the observed TC center than that without filtering (Figures 1(a) and 1(b)) on 1200 UTC 30 July 2008. The distance between observed TC center and that determined by simulated SLP is about 28 km and is slightly less than the distance (29 km) determined using 850 hPa geopotential height. It is clear that SLP and 850 hPa geopotential height have fair performance to identify the landed TC center in simulation. Analyzing the performance of different methods of identifying TC center is beyond the scope of the present paper. Therefore, we will focus on the subsequent section on the comparative analysis with or without Barnes filter based on SLP.

The observed and simulated tracks of typhoon Fung-Wong after landing China are depicted in Figure 3(b). The WRF model well simulates the movement of TC Fung-Wong after landing China. The distances between the simulated TC centers determined by filtered SLP with (open circle in Figure 3(b)) and without Barnes filter (filled circle in Figure 3(b)) are usually small (less than 30 km). But at 1200 UTC 29 July, 0600 UTC 30 July, and 1200 UTC 30 July, the distances are greater than 40 km (especially for 1200 UTC 30 July, the distance is up to 100 km) and the TC center determined by filtered SLP is much closer to the observation. This implies that most of the times the TC center identified by SLP filtered with Barnes filter is consistent with that without Barnes filter, but in a few times there are significant differences between the two centers (with or without Barnes filter) due to the presence of small-scale perturbations in SLP.

4.2. Statistical Analysis. Above case study indicates that, before identifying TC center from numerical models, first

Table 1: The TCs landing Chinese mainland during 2005 to 2015.

TC number	Name of TC	Start time	End time
200509	Matsa	2005080518	2005080718
200510	Sanvu	2005081300	2005081500
200515	Khanun	2005091108	2005091308
200606	Prapiroon	2006080306	2006080506
200713	Wipha	2007091818	2007092018
200807	Kalmaegi	2008071806	2008072006
200808	Fung-Wong	2008072812	2008073012
201211	Haikui	2012080718	2012080918
201311	Utor	2013081406	2013081606
201312	Trami	2013082118	2013082318
201410	Matmo	2014072306	2014072506
201513	Soudelor	2015080812	2015081012

removing the small-scale perturbations with wavelength less than 100 km using Barnes filter can effectively promote the accuracy of simulated TC center. In order to verify whether this holds in a statistical sense, 12 TCs (Table 1) which landed Chinese mainland from 2005 to 2015 and survived at least 36 h over land are simulated by WRF V3.6. The model domain and physical configures are the same as that of the case study in Section 2, except for the start time and end time which are listed in Table 1 for each TC. Then the simulated SLP for each TC is filtered by Barnes filter with $C = 2500$ and $G = 0.35$ to remove the small-scale perturbations with wavelength less than 100 km. Using the method of the lowest SLP, two groups of TC tracks (centers) are obtained from model output SLP (i.e., without Barnes filter) and filtered SLP with Barnes filter (i.e., with Barnes filter), respectively.

Moreover, the corresponding statistical analysis of two groups of TC centers is carried out by estimating the distance between them. The distance D is calculated by the formula as

$$D = R \cdot \arccos\left(\cos\varphi_1 \cos\varphi_2 \cos\left(\theta_1 - \theta_2\right) + \sin\varphi_1 \cos\varphi_2\right), \quad (7)$$

where θ_1 and φ_1 are the longitude and latitude of TC center obtained from SLP without Barnes filter and θ_2 and φ_2 are the longitude and latitude of TC center obtained from SLP with Barnes filter. The frequency variation of 118 distances corresponding to 12 TCs is shown in Figure 4. As can be seen from Figure 4, the frequency rapidly decreases with the increase of distance. Specifically, among 118 distances, there are 96 (51.1%) distances less than 20 km, 40 (21.3%) distances between 20 and 30 km, 24 (12.8%) distances between 30 and 40 km, and 28 (14.8%) distances more than 40 km. It is clear that the most (about 85%) of distances between the TC center obtained from SLP with and without Barnes filter are within 40 km. It further indicates that, in most cases, regardless of model output SLP which is filtered by Barnes filter or not to remove small-scale perturbations with wavelength less than 100 km, the SLP can correctly determine the TC center. But in few cases (about 15%), directly using model output SLP to identify the center can result in large deviation from that using filtering.

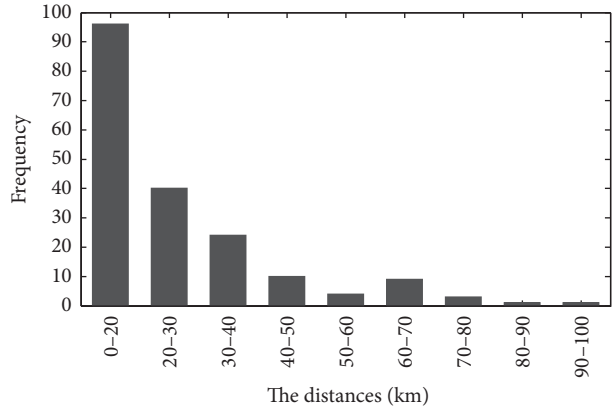

Figure 4: The histogram of distances between the TC centers obtained from SLP with and without Barnes filter.

In a few cases (about 15%), there are large distances between the TC centers obtained from SLP with and without Barnes filter. Which one is closer to the observed TC center? To address this problem, the distance difference (DD) between the TC center obtained from SLP with or without Barnes filter and observed TC centers is introduced as

$$\begin{aligned} \mathrm{DD} &= D_1 - D_2, \\ D_1 &= R \cdot \arccos\left(\cos\varphi_1 \cos\varphi_o \cos\left(\theta_1 - \theta_o\right) + \sin\varphi_1 \cos\varphi_o\right), \\ D_2 &= R \cdot \arccos\left(\cos\varphi_2 \cos\varphi_o \cos\left(\theta_2 - \theta_o\right) + \sin\varphi_2 \cos\varphi_o\right), \end{aligned} \quad (8)$$

where θ_o and φ_o are the longitude and latitude of observed TC center, respectively. Figure 5 describes the frequency variation of DDs associated with 12 TCs. We can see from Figure 5 that the high frequency of DDs locates between −30 km and 30 km, accounting for 85.4%. Moreover, DDs almost fairly distribute at −30~0 km (40.4%) and 0~30 km (45.0%). This also indicates that, in most cases (about 85%), whether the SLP field is filtered by Barnes filter or not

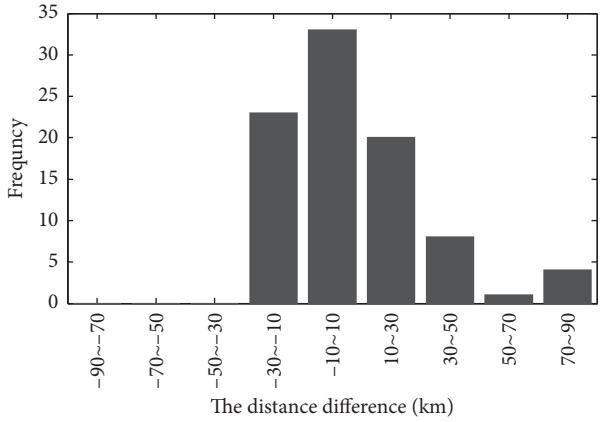

Figure 5: The histogram of the distance difference (DD) between the TC centers obtained from SLP with Barnes filter or without Barnes filter and that from best-track data.

for removing small-scale perturbations with wavelength less than 100 km has no obvious effect on finding TC center in numerical models. More importantly, as also shown in Figure 5 that there is no one case with DD less than −30 km, cases with DD more than 30 km appear 13 times, which accounts for 14.6% and is similar to that of D more than 40 km in Figure 4. The cases with DD more than 70 km even happen 4 times, accounting for 5.0%. This implies that, in few cases (about 15%), removing the small-scale perturbations with wavelength less than 100 km in SLP field based on Barnes filter can correctly identify the simulated TC center while the directly model output SLP cannot. Figure 5 shows that DDs sometimes show negative values. Why do the negative values appear? Actually, the small-scale perturbations may stochastically present within the main body of TC. For example, at 0600 UTC 30 July 2014 when the TC Matmo landed China, two obvious small-scale perturbations with simulated SLP less than 991.5 hPa appeared at the eastern and western sides of the main body (i.e., the isoline of 993 hPa) of Matmo (Figure 6(a)). The small-scale perturbation in the west is stronger than that in the east, resulting in the TC center within the west small-scale perturbation. Meanwhile, since the observed TC center also locates at the western of the main body of Matmo, the distance between observed TC center and simulated TC center obtained from SLP without Barnes filter is shorter than that with Barnes filter. This results in negative DD. In fact, if the stronger small-scale perturbation locates at the eastern of main body of TC rather than western (this situation actually happens at UTC 0500 30 July 2014, i.e., 1 h prior to Figure 6(a)), the simulated TC center obtained from SLP without Barnes filter locates within the east small-scale perturbation (Figure 6(b)). This results in positive DD. Therefore, the negative values of DDs are mainly responsible for the fact that the small-scale perturbations present irregularly within the main body of the TC vortex. Besides, the performance of the model and the accuracy of the best-track data also affect DD in a certain extent. Comparing Figure 6(a) with Figure 6(b), the TC center obtained from SLP without Barnes filter travels about 100 km in 1 h from 0500 to 0600 UTC 30 July 2014. In contrast, the TC center determined by Barnes filter only travels about 20 km. The latter is more smooth and reasonable and is much close to the movement speed of observed TC. Therefore, although sometimes the DDs are negative, the TC center obtained from SLP with Barnes filter performs overall better than that without Barnes filter because of the large number of positive DD values (Figure 5, the average of DDs is positive) and smooth tracks (i.e., small translating speed of TC center). Clearly, using the SLP field processed with Barnes filter to remove small-scale perturbations instead of using the model output SLP directly can effectively improve the accuracy of positioning TC centers (track) in numerical model after TC making landfall.

5. Conclusions

After TC landed mainland, its intensity rapidly weakens due to the large friction and the reduction of water vapor supply. In the presence of heterogeneous land surface, some small-scale perturbations with wavelength less than 100 km appear around the true TC center in numerically simulated SLP field. This often results in the failure of identifying the TC center based on the lowest SLP. A classical scale separation tool named Barnes filter is introduced to fix the problem. The suitable weight function coefficients C and G for removing these small-scale perturbations (wavelength less than 100 km) and meanwhile preserving TC signals are set to 2500 and 0.35, respectively.

The Barnes filter with $C = 2500$ and $G = 0.35$ is applied in the simulated SLP field of TC Fong-Wang when it traveled over Chinese mainland from 1500 UTC 28 to 1200 UTC 30 July 2008. The results show that the Barnes filter not only cleanly removes the small-scale perturbations with wavelength less than 100 km, but also perfectly preserves the signals of TC. The corresponding TC centers (track) determined by SLP filtered with Barnes filter using the lowest SLP are much closer to the observed TC centers (track), as compared to that identified without filtering. Twelve TCs which landed Chinese mainland from 2005 to 2015 are simulated and then the output SLP field is processed by Barnes filter to remove small-scale perturbations. Two groups of TC centers are obtained from model output SLP with and without Barnes filtering, respectively. The statistics analysis of the two groups of TC centers compared to the observed ones is performed based on the DD (distance difference: the distance between TC center determined by SLP without Barnes filter and observed TC center minus that with Barnes filter). Results show that in most cases (about 85%) the DDs are small (between −30 km and 30 km), while in a few cases (about 15%) the DDs are large (greater than 30 km even 70 km). This further implies that the TC centers determined by SLP with Barnes filter are overall more accurate than that from direct model output SLP. Moreover, the TC track with Barnes filter is much smoother than that without Barnes filter.

Using Barnes filter to remove small-scale perturbations with wavelength less than 100 km from model output SLP field, the simulated TC center can be commendably identified after a TC making landfall. It should be noted that this study focus on the action of Barnes filter. But the methods to identify landed TC center from model output variables processed

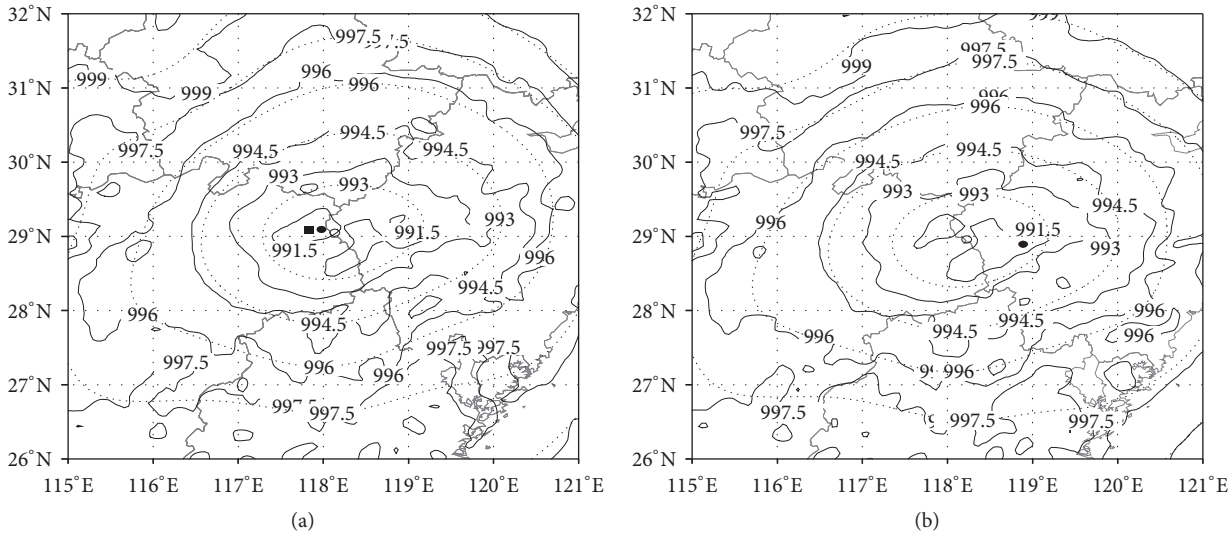

Figure 6: The simulated SLP (unit hPa) field with Barnes filter (dotted lines) and without Barnes filter (solid lines) for (a) 0600 UTC and (b) 0500 UTC 24 July 2014 after TC Matmo landed China. Open (filled) circle indicates the TC center determined by SLP with (without) Barnes filter. Filled square represents the observed TC center.

by Barnes filter, such as the centroid pressure method, the centroid vorticity method, and the lowest geopotential height method, are also important. Future study should focus on the comparing analysis of different methods in identifying simulated TC center from different model output variables which has processed by Barnes filter.

Conflicts of Interest

The authors declare that they have no conflicts of interest.

Acknowledgments

This study is jointly supported by Jiangxi Provincial Department of Science and Technology Project (Grant no. 20171BBG70004), the Special Scientific Research Fund of Meteorological Public Welfare Profession of China (Grant no. GYHY201506002), and the National Natural Science Foundation of China (Grant no. 41765001).

References

[1] P.-L. Chang, B. J.-D. Jou, and J. Zhang, "An algorithm for tracking eyes of tropical cyclones," *Weather and Forecasting*, vol. 24, no. 1, pp. 245–261, 2009.

[2] S. Chaurasia, C. M. Kishtawal, and P. K. Pal, "An objective method of cyclone centre determination from geostationary satellite observations," *International Journal of Remote Sensing*, vol. 31, no. 10, pp. 2429–2440, 2010.

[3] C. W. Landsea and Coauthors, "The Atlantic hurricane database re-analysis project: Documentation for the 1851-1910 alterations and additions to the HURDAT database," in *Hurricanes and Typhoons: Past, Present and Future*, R. J. Murnane and and K.-B. Liu, Eds., pp. 177–221, Columbia University Press, 2004.

[4] A. J. Wimmers and C. S. Velden, "Objectively determining the rotational center of tropical cyclones in passive microwave satellite imagery," *Journal of Applied Meteorology and Climatology*, vol. 49, no. 9, pp. 2013–2034, 2010.

[5] Z. Mingjian, Y. Bo, W. Haiying et al., "Researches and Applications of Locating Technology for Typhoon Center of Satellite Infrared Cloud Picture," *Journal of Tropical Meteorology*, vol. 22, no. 3, pp. 241–247, 2006.

[6] J. S. Goerss, "Impact of satellite observations on the tropical cyclone track forecasts of the navy operational global atmospheric prediction system," *Monthly Weather Review*, vol. 137, no. 1, pp. 41–50, 2009.

[7] S. D. Aberson, "Two years of operational hurricane synoptic surveillance," *Weather and Forecasting*, vol. 17, no. 5, pp. 1101–1110, 2002.

[8] Z. Liu, E. R. Dougherty, J. T. Astola et al., "Automatic center location of non-eyed typhoon in satellite cloud image," in *Proceedings of the Electronic Imaging 2003*, p. 429, Santa Clara, CA.

[9] J. D. Kepert, "Objective analysis of tropical cyclone location and motion from high-density observations," *Monthly Weather Review*, vol. 133, no. 8, pp. 2406–2421, 2005.

[10] V. T. Wood, "A technique for detecting a tropical cyclone center using a Doppler radar," *Journal of Atmospheric and Oceanic Technology*, vol. 11, no. 5, pp. 1207–1216, 1994.

[11] W.-C. Lee, B. J.-D. Jou, P.-L. Chang, and S.-M. Deng, "Tropical cyclone kinematic structure retrieved from single-doppler radar observations. Part I: Interpretation of Doppler velocity patterns and the GBVTD technique," *Monthly Weather Review*, vol. 127, no. 10, pp. 2419–2439, 1998.

[12] X. Ying-Long, J. Mei-Yan, B. Bao-Gui et al., "The Applied Study of the Positioning Method of a Tropical Cyclone over Offshore Using a Doppler Radar," *Chinese Journal of Atmospheric Sciences*, vol. 30, no. 6, pp. 1119–1128, 2006 (Chinese).

[13] H. V. Senn and H. W. O. Hiser, "the Origin of Hurricane Spiral Rain Bands," *Journal of the Atmospheric Sciences*, vol. 16, no. 4, pp. 419–426, 2010.

[14] M. M. Bell and W.-C. Lee, "Objective tropical cyclone center tracking using single-doppler radar," *Journal of Applied Meteorology and Climatology*, vol. 51, no. 5, pp. 878–896, 2011.

[15] Z. Yong, L. Liping, Z. Zhiqiang et al., "Typhoon Location in Landing Period Based on Three Dimensional Mosaics of Reflectivity," *Meteorological Science and Technology*, vol. 39, no. 5, pp. 587–595, 2011.

[16] M. Ying, W. Zhang, H. Yu et al., "An overview of the China meteorological administration tropical cyclone database," *Journal of Atmospheric and Oceanic Technology*, vol. 31, no. 2, pp. 287–301, 2014.

[17] C. Velden, B. Harper, F. Wells et al., "The Dvorak tropical cyclone intensity estimation technique: A satellite-based method that has endured for over 30 years," *Bulletin of the American Meteorological Society*, vol. 87, no. 9, pp. 1195–1210, 2006.

[18] J. H. Cossuth, R. D. Knabb, D. P. Brown, and R. E. Hart, "Tropical cyclone formation guidance using pregenesis dvorak climatology. Part I: Operational forecasting and predictive potential," *Weather and Forecasting*, vol. 28, no. 1, pp. 100–118, 2012.

[19] V. F. Dvorak, "Tropical Cyclone Intensity Analysis and Forecasting from Satellite Imagery," *Monthly Weather Review*, vol. 103, no. 5, pp. 420–430, 1975.

[20] V. F. Dvorak, "Tropical cyclone intensity analysis using satellite data," NOAA Tech. Rep, 1984.

[21] V. F. Dvorak, *Tropical clouds and cloud systems observed in satellite imagery: Tropical cyclones. Workbook*, vol. 2, 1995.

[22] X. Li, "Sensitivity of WRF simulated typhoon track and intensity over the Northwest Pacific Ocean to cumulus schemes," *Science China Earth Sciences*, vol. 56, no. 2, pp. 270–281, 2012.

[23] Z. Shuixin, C. Zitong, D. Guangfeng et al., "Impacts of Orographic Gravity Wave Drag Parameterization on Typhoon Intensity and Path Forecasting," *Chinese Journal of Atmospheric Sciences*, vol. 38, no. 2, pp. 273–284, 2014 (Chinese).

[24] F. T. Cruz and G. T. Narisma, "WRF simulation of the heavy rainfall over Metropolitan Manila, Philippines during tropical cyclone Ketsana: a sensitivity study," *Meteorology and Atmospheric Physics*, vol. 128, no. 4, pp. 415–428, 2016.

[25] M. Fiorino, J. S. Goerss, J. J. Jensen, and E. J. Harrison Jr., "An evaluation of the real-time tropical cyclone forecast skill of the navy operational global atmospheric prediction system in the western North Pacific," *Weather & Forecasting*, vol. 8, no. 1, pp. 3–24, 1993.

[26] L.-F. Hsiao, C.-S. Liou, T.-C. Yeh et al., "A vortex relocation scheme for tropical cyclone initialization in advanced research WRF," *Monthly Weather Review*, vol. 138, no. 8, pp. 3298–3315, 2010.

[27] J. T. Heming, J. C. L. Chan, and A. M. Radford, "A new scheme for the initialisation of tropical cyclones in the UK Meteorological Office global model," *Meteorological Applications*, vol. 2, no. 2, pp. 171–184, 1995.

[28] C.-S. Liou and K. D. Sashegyi, "On the initialization of tropical cyclones with a three dimensional variational analysis," *Natural Hazards*, vol. 63, no. 3, pp. 1375–1391, 2012.

[29] L. T. Nguyen, J. Molinari, and D. Thomas, "Evaluation of tropical cyclone center identification methods in numerical models," *Monthly Weather Review*, vol. 142, no. 11, pp. 4326–4339, 2014.

[30] Y. Kurihara, R. E. Tuleya, and M. A. Bender, "The GFDL Hurricane Prediction System and its performance in the 1995 hurricane season," *Monthly Weather Review*, vol. 126, no. 5, pp. 1306–1322, 1998.

[31] Lord and R. A. Petersen, "Hurricane track forecasts using synthetic data in the NMC Global Analysis and Forecast System," in *Proceedings of the WMO Tech. Conf. on Tropical Aeronautical Meteorology (TECTAM-92)*, WMO, Geneva, Switzerland, 1993.

[32] K. Walsh, "Objective detection of tropical cyclones in high-resolution analyses," *Monthly Weather Review*, vol. 125, no. 8, pp. 1767–1779, 1997.

[33] S. L. Barnes, "A technique for maximizing details in numerical weather map analysis," *Journal of Applied Meteorology and Climatology*, vol. 3, no. 4, pp. 396–409, 1964.

[34] S. L. Barnes, "Mesoscale objective map analysis using weighted time series observations," *NOAA Technical Memorandum*, pp. 62-60, 1973.

[35] C. A. Doswell, "Obtaining Meteorologically Significant Surface Divergence Fields Through the Filtering Property of Objective Analysis," *Monthly Weather Review*, vol. 105, no. 7, pp. 885–892, 1977.

[36] D. Gomis and S. Alonso, "Diagnosis of a cyclogenetic event in the western Mediterranean using an objective technique for scale separation," *Monthly Weather Review*, vol. 118, no. 3, pp. 723–736, 1990.

[37] Z. Hong, L. Guoping, and W. Shudong, "Mesoscale Filtering Analysisi of a Regional Heavy Rain by Southwest Vortex," *Plateau Meteorology*, vol. 33, no. 2, pp. 361–371, 2014.

[38] M. A. Askelson, J.-P. Aubagnac, and J. M. Straka, "An adaptation of the Barnes filter applied to the objective analysis of radar data," *Monthly Weather Review*, vol. 128, no. 9, pp. 3050–3082, 2000.